# Training a Feedback Loop for Hand Pose Estimation

Markus Oberweger      Paul Wohlhart      Vincent Lepetit

Institute for Computer Graphics and Vision

Graz University of Technology, Austria

`{oberweger,wohlhart,lepetit}@icg.tugraz.at`

## Abstract

*We propose an entirely data-driven approach to estimating the 3D pose of a hand given a depth image. We show that we can correct the mistakes made by a Convolutional Neural Network trained to predict an estimate of the 3D pose by using a feedback loop. The components of this feedback loop are also Deep Networks, optimized using training data. They remove the need for fitting a 3D model to the input data, which requires both a carefully designed fitting function and algorithm. We show that our approach outperforms state-of-the-art methods, and is efficient as our implementation runs at over 400 fps on a single GPU.*

## 1. Introduction

Accurate hand pose estimation is an important requirement for many Human Computer Interaction or Augmented Reality tasks [10], and has been steadily regaining ground as a focus of research interest in the past few years [13, 14, 19, 23, 26, 30, 31, 37], probably because of the emergence of 3D sensors. Despite 3D sensors, however, it is still a very challenging problem, because of the vast range of potential freedoms it involves, and because images of hands exhibit self-similarity and self-occlusions.

A popular approach is to use a discriminative method to predict the position of the joints [13, 21, 30, 31, 35], because they are now robust and fast. To refine the pose further, they are often used to initialize an optimization where a 3D model of the hand is fit to the input depth data [1, 8, 23, 24, 26, 28, 29, 36]. Such an optimization remains complex, however, and typically requires the maintaining of multiple hypotheses [22, 23, 26]. It also relies on a criterion to evaluate how well the 3D model fits to the input data, and designing such a criterion is not a simple and straightforward task [1, 8, 29].

In this paper, we first show how we can get rid of the 3D model of the hand altogether and build instead upon recent work that learns to generate images from training data [9]. We then introduce a method that learns to provide updates
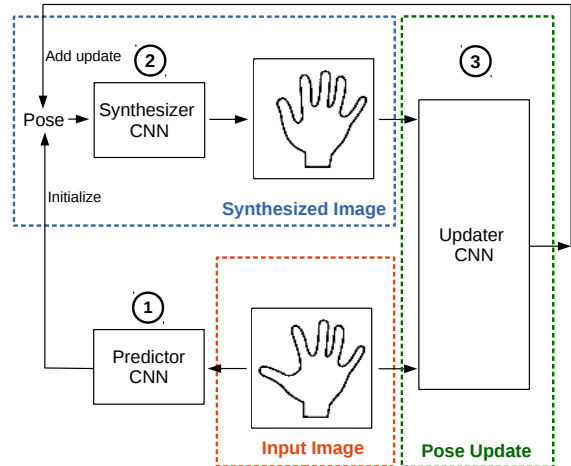


Figure 1: Overview of our method. We use a first CNN ① to predict an initial estimate of the 3D pose given an input depth image of the hand. The pose is used to synthesize an image ②, which is used together with the input depth image to derive a pose update ③. The update is applied to the pose and the process is iterated.

for improving the current estimate of the pose, given the input image and the image generated for this pose estimate as shown in Fig. 1. By iterating this method a number of times, we can correct the mistakes of an initial estimate provided by a simple discriminative method. All the components are implemented as Deep Networks with simple architectures.

Not only is it interesting to see that all the components needed for hand registration that used to require careful design can be learned instead, but we will also show that our approach has superior performance when compared to the state-of-the-art methods. It is also efficient; our implementation runs at over 400 fps on a single GPU.

Our approach is related to generative approaches [3], in particular [32] which also features a feedback loop reminiscent of ours. However, our approach is deterministic and does not require an optimization based on distribution sampling, on which generative approaches generally rely, but which tend to be inefficient.

1

## 2. Related Work

Hand pose estimation is a frequently visited problem in Computer Vision, and is the subject of a plethora of published work. We refer to [10] for an overview of earlier work, and here we will discuss only more recent work, which can be divided into two types of approach.

The first type of approach is based on discriminative models that aim at directly predicting the joint locations from RGB or RGB-D images. Some recent works include [13, 14, 17, 30, 31] that use different approaches with Random Forests, but restricted to static gestures, showing difficulties with occluded joints, or causing high inaccuracies at finger tips. These problems have been addressed by more recent works of [21, 35] that use Convolutional Neural Networks, nevertheless still lacking in high accuracy levels.

Our approach, however, is more related to the second type, which covers generative, model-based methods. The works of this type are developed from four generic building blocks: (1) a hand model, (2) a similarity function that measures the fit of the observed image to the model, (3) an optimization algorithm that maximizes the similarity function with respect to the model parameters, and (4) an initial pose from which the optimization starts.

For the hand model, different hand-crafted models were proposed. The choice of a simple model is important for maintaining real-time capabilities, and representing a trade-off between speed and accuracy as a response to a potentially high degree of model abstraction. Different hand-crafted geometrical approximations for hand models were proposed. For example, [26] uses a hand model consisting of spheres, [23] adds cylinders, ellipsoids, and cones. [29] models the hand from a Sum of Gaussians. More holistic hand representations are used by [1, 28, 36], with a linear blend skinning model of the hand that is rendered as depth map. [37] increases the matching quality by using depth images that resemble the same noise pattern as the depth sensor. [8] uses a fully shaded and textured triangle mesh controlled by a skeleton.

Different modalities were proposed for the similarity function, which are coupled to the used model. The modalities include, *e.g.*, depth values [19, 22, 26], salient points, edges, color [8], or combinations of these [1, 23, 29, 36].

The optimization of the similarity function is a critical part, as the high dimensional pose space is prone to local minima. Thus, Particle Swarm Optimization is often used to handle the high dimensionality of the pose vector [22, 23, 26, 28]. Differently, [1, 8, 29] use gradient-based methods to optimize the pose, while [19] uses dynamics simulation. Due to the high computation time of these optimization methods, which have to be solved for every frame, [37] does not optimize the pose but only evaluates the similarity function for several proposals to select the best fit.

In order to kick-start optimization, [29] uses a discriminative part-based pose initialization, and [26] uses finger tips only. [37] predicts candidate poses using a Hough Forest. [8] requires predefined hand color and position, and [23] relies on a manual initialization. Furthermore, tracking-based methods use the pose of the last frame [19, 23, 36], which can be problematic if the difference between frames is too large, because of fast motion or low frame rates.

Our approach differs from previous work in the first three building blocks. We do not use a deformable CAD model of the hand. Instead, we learn from registered depth images to generate realistic depth images of hands, similar to work on inverse graphics networks [9, 15], and other recent work on generating images [11, 16]. This approach is very convenient, since deforming correctly and rendering a CAD model of the hand in a realistic manner requires a significant input of engineering work.

In addition, we do not use a hand-crafted similarity function and an optimization algorithm. We learn rather to predict updates that improve the current estimate of the hand pose from training data, given the input depth image and a generated image for this estimate. Again this approach is very convenient, since it means we do not need to design the similarity function and the optimization algorithm, neither of which is a simple task.

Since we learn to generate images of the hand, our approach is also related to generative approaches, in particular [32]. It uses a feedback loop with an updater mechanism akin to ours. It predicts updates for the position from which a patch is cropped from an image, such that the patch fits best to the output of a generative model. However, this step does not predict the full set of parameters. The hidden states of the model are found by a costly sampling process.

[20] relies on a given black-box image synthesizer to provide synthetic samples on which the regression network can be trained. It then learns a network to substitute the black-box graphics model, which can ultimately be used to update the pose parameters to generate an image that most resembles the input. In contrast, we learn the generator model directly from training data, without the need for a black-box image synthesizer. Moreover, we will show that the optimization is prone to output infeasible poses or get stuck in local minima and therefore introduce a better approach to improve the pose.

## 3. Model-based Pose Optimization

In this section, we will first give an overview of our method. We then describe in detail the different components of our method: A discriminative approach to predict a first pose estimate, a method able to generate realistic depth images of the hand, and a learning-based method to refine the initial pose estimate using the generated depth images.
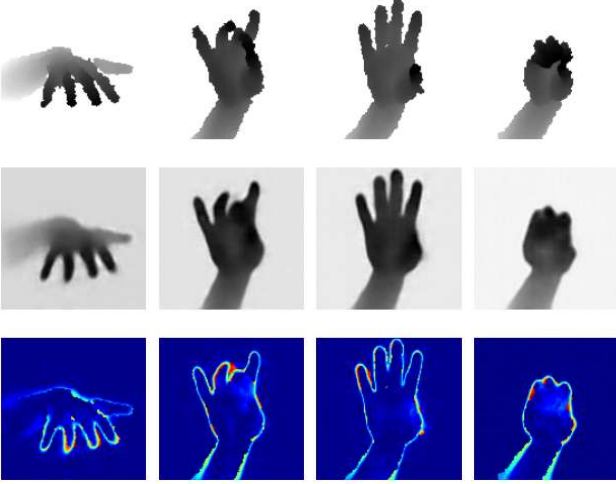
Figure 2: Samples generated by the synthesizer for different poses from the test set. **Top:** Ground truth depth image. **Middle:** Synthesized depth image using our learned hand model. **Bottom:** Color-coded, pixel-wise difference between the depth images. The synthesizer is able to render convincing depth images for a very large range of poses. The largest errors are located near the occluding contours of the hand, which are noisy in the ground truth images. (Best viewed on screen)

## 3.1. Method Overview

Our objective is to estimate the pose $\mathbf{p}$ of a hand in the form of the 3D locations of its joints $\mathbf{p} = \{\mathbf{j}_i\}_{i=1}^J$ with $\mathbf{j}_i = (x_i, y_i, z_i)$ from a single depth image $\mathcal{D}$. In practice, $J = 14$ for the dataset we use. We assume that a training set $\mathcal{T} = \{(\mathcal{D}_i, \mathbf{p}_i)\}_{i=1}^N$ of depth images labeled with the corresponding 3D joint locations is available.

As explained in the introduction, we first train a predictor to predict an initial pose estimate $\widehat{\mathbf{p}}^{(0)}$ in a discriminative manner given an input depth image $\mathcal{D}_{\text{input}}$:

$$\widehat{\mathbf{p}}^{(0)} = \text{pred}(\mathcal{D}_{\text{input}}) \ . \tag{1}$$

We use a Convolutional Neural Network (CNN) to implement the $\text{pred}(.)$ function with a standard architecture. More details will be given in Section 3.2.

In practice, $\widehat{\mathbf{p}}^{(0)}$ is never perfect, and following the motivation provided in the introduction, we introduce a hand model learned from the training data. As shown in Fig. 2, this model can synthesize the depth image corresponding to a given pose $\mathbf{p}$, and we will refer to this model as the *synthesizer*:

$$\mathcal{D}_{\text{synth}} = \text{synth}(\mathbf{p}) \ . \tag{2}$$

We also use a Deep Network to implement the synthesizer.

A straightforward way of using this synthesizer would consist in estimating the hand pose $\widehat{\mathbf{p}}$ by minimizing the
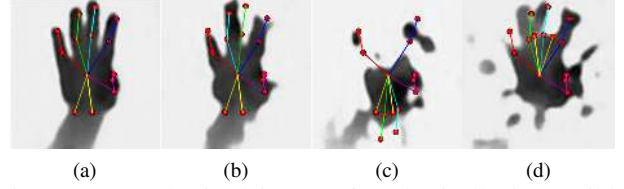


Figure 3: Synthesized images for physically impossible poses. Note the colors that indicate different fingers. (a) shows a feasible pose with its synthesized image. (b) shows the synthesized image for the same pose after swapping the ring and middle finger positions. In (c) the ring and middle finger are flipped downwards, and in (d) the wrist joints are flipped upwards. (Best viewed on screen)

squared loss between the input image and the synthetic one:

$$\widehat{\mathbf{p}} = \arg\min_{\mathbf{p}} \|\mathcal{D}_{\text{input}} - \text{synth}(\mathbf{p})\|^2 \ . \tag{3}$$

This is a non-linear least-squares problem, which can be solved iteratively using $\widehat{\mathbf{p}}^{(0)}$ as initial estimate. However, the objective function of Eq. (3) exhibits many local minima. Moreover, during the optimization of Eq. (3), $\mathbf{p}$ can take values that correspond to physically infeasible poses. For such values, the output $\text{synth}(\mathbf{p})$ of the synthesizer is unpredictable as depicted in Fig. 3, and this is likely to make the optimization of Eq. (3) diverge or be stuck in a local minimum, as we will show in the experiments in Section 4.5.

We therefore introduce a third function that we call the $\text{updater}(.,.)$. It learns to predict updates, which are applied to the pose estimate to improve it, given the input image $\mathcal{D}_{\text{input}}$ and the image $\text{synth}(\mathbf{p})$ produced by the synthesizer:

$$\widehat{\mathbf{p}}^{(i+1)} \leftarrow \widehat{\mathbf{p}}^{(i)} + \text{updater}(\mathcal{D}_{\text{input}}, \text{synth}(\widehat{\mathbf{p}}^{(i)})) \ . \tag{4}$$

We iterate this update several times to improve the initial pose estimate. Again, the $\text{updater}(.,.)$ function is implemented as a Deep Network.

We detail below how we implement and train the $\text{pred}(.)$, $\text{synth}(.)$ and $\text{updater}(.,.)$ functions.

## 3.2. Learning the Predictor Function $\text{pred}(.)$

The predictor is implemented as a CNN. The network consists of a convolutional layer with $5 \times 5$ filter kernels producing 8 feature maps. These feature maps are max-pooled with $4 \times 4$ windows, followed by a hidden layer with 1024 neurons and an output layer with one neuron for each joint and dimension, *i.e.* $3 \cdot J$ neurons. The predictor is parametrized by $\Phi$, which is obtained by minimizing

$$\widehat{\Phi} = \arg\min_{\Phi} \sum_{(\mathcal{D}, \mathbf{p}) \in \mathcal{T}} \|\text{pred}_{\Phi}(\mathcal{D}) - \mathbf{p}\|_2^2 + \gamma \|\Phi\|_2^2 \ , \tag{5}$$

where the second term is a regularizer for weight decay with $\gamma = 0.001$.

### 3.3. Learning the Synthesizer Function synth(.)

We use a CNN to implement the synthesizer, and we train it using the set $\mathcal{T}$ of annotated training pairs. The network architecture is strongly inspired by [9], and is shown in Fig. 4. It consists of four hidden layers, which learn an initial latent representation of feature maps apparent after the fourth fully connected layer FC4. These latent feature maps are followed by several unpooling and convolution layers. The unpooling operation, used for example by [9, 11, 38, 39], is the inverse of the max-pooling operation: The feature map is expanded, in our case by a factor of 2 along each image dimension. The emerging "holes" are filled with zeros. The expanded feature maps are then convolved with trained 3D filters to generate another set of feature maps. These unpooling and convolution operations are applied subsequently. The last convolution layer combines all feature maps to generate a depth image.

We learn the parameters $\widehat{\Theta}$ of the network by minimizing the difference between the generated depth images $\mathrm{synth}(\mathbf{p})$ and the training depth images $\mathcal{D}$ as

$$\widehat{\Theta} = \arg\min_{\Theta} \sum_{(\mathcal{D},\mathbf{p})\in\mathcal{T}} \frac{1}{|\mathcal{D}|} \|\mathrm{synth}_{\Theta}(\mathbf{p}) - \mathcal{D}\|_2^2 \ . \quad (6)$$

We perform the optimization in a layer-wise fashion. We start by training the first $8 \times 8$ feature map. Then we gradually extend the output size by adding another unpooling and convolutional layer and train again, which achieves lesser errors than end-to-end training in our experience.

The synthesizer is able to generate accurate images, maybe surprisingly well for such a simple architecture. The median pixel error on the test set is only 1.3 mm. However, the average pixel error is $10.9\pm32.2mm$. This is mostly due to noise in the input images along the outline of the hand, which is smoothed away by the synthesizer. The average depth accuracy of the sensor is $\pm1\ mm$ [25].

### 3.4. Learning the Updater Function updater(.,.)

The updater function $\mathrm{updater}(.,.)$ takes two depth images as input. As already stated in Eq. (4), at run-time, the first image is the input depth image, the second image is the image returned by the synthesizer for the current pose estimate. Its output is an update that improves the pose estimate. The architecture, shown in Fig. 5, is inspired by the Siamese network [6]. It consists of two identical paths with shared weights. One path is fed with the observed image and the second path is fed with the image from the synthesizer. Each path consists of four convolutional layers. We do not use max-pooling here, but a filter stride [12, 18] to reduce the resolution of the feature maps. We experienced inferior accuracy with max-pooling compared to that with stride, probably because max-pooling introduces spatial invariance [27] that is not desired for this task. The feature
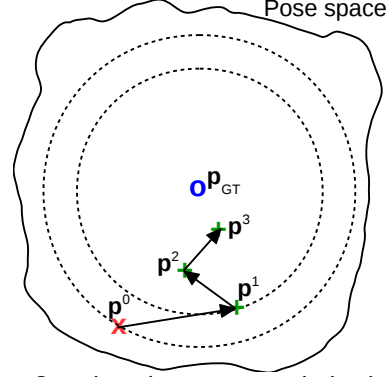


Figure 6: Our iterative pose optimization in high-dimensional space, schematized here in 2D. We start at an initial pose ($\times$) and want to converge to the ground truth pose ($\circ$), that maximizes image similarity. Our predictor generates updates for each pose ($+$) that bring us closer. The updates are predicted from the synthesized image of the current pose estimate and the observed depth image. (Best viewed in color)

maps of the two paths are concatenated and fed into a fully connected network that outputs the update.

Ideally, the output of the updater should bring the pose estimate to the correct pose in a single step. However, this is a very difficult problem, and we could not get the network to reduce the initial training error within a reasonable timeframe. However, our only requirement from the updater is for it to output an update which brings us closer to the ground truth as shown in Fig. 6. We iterate this update procedure to get closer step-by-step. Thus, the update should follow the inequality

$$\|\mathbf{p} + \mathrm{updater}(\mathcal{D}, \mathrm{synth}(\mathbf{p})) - \mathbf{p}_{\mathrm{GT}}\|_2 < \lambda\|\mathbf{p} - \mathbf{p}_{\mathrm{GT}}\|_2 \ , \quad (7)$$

where $\mathbf{p}_{\mathrm{GT}}$ is the ground truth pose for image $\mathcal{D}$, and $\lambda \in [0, 1]$ is a multiplicative factor that specifies a minimal improvement. We use $\lambda = 0.6$ in our experiments.

We optimize the parameters $\Omega$ of the updater by minimizing the following cost function

$$\mathcal{L} = \sum_{(\mathcal{D},\mathbf{p})\in\mathcal{T}} \sum_{\mathbf{p}'\in\mathcal{T}_{\mathcal{D}}} \max(0, \|\mathbf{p}''-\mathbf{p}\|_2 - \lambda\|\mathbf{p}'-\mathbf{p}\|_2) \ , \quad (8)$$

where $\mathbf{p}'' = \mathbf{p}' + \mathrm{updater}_{\Omega}(\mathcal{D}, \mathrm{synth}(\mathbf{p}'))$, and $\mathcal{T}_{\mathcal{D}}$ is a set of poses. The introduction of the synthesizer allows us to virtually augment the training data and add arbitrary poses to $\mathcal{T}_{\mathcal{D}}$, which the updater is then trained to correct.

The set $\mathcal{T}_{\mathcal{D}}$ contains the ground truth $\mathbf{p}$, for which the updater should output a zero update. We further add as many meaningful deviations from that ground truth as possible, which the updater might perceive during testing and be asked to correct. We start by including the output pose of the predictor $\mathrm{pred}(\mathcal{D})$, which during testing is used as initialization of the update loop. Additionally, we add copies
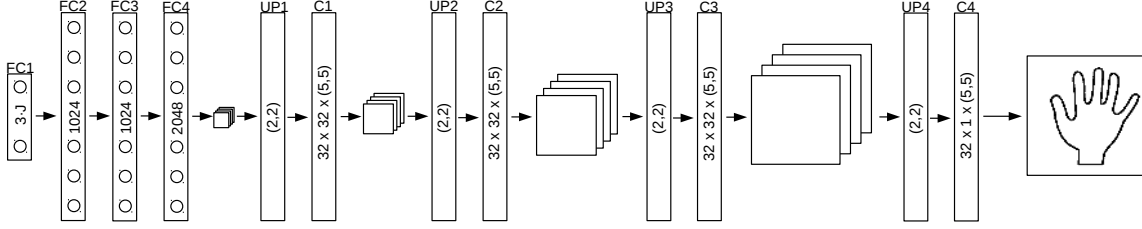
Figure 4: Network architecture of the synthesizer used to generate depth images of hands given their poses. The input of the network is the hand pose. The fully connected hidden layers create a 2048 dimensional latent representation at FC4 which is reshaped into 32 feature maps of size $8 \times 8$. The feature maps are gradually enlarged by successive unpooling and convolution operations. The last convolution layer combines the feature maps to derive a single depth image of size $128 \times 128$. All layers have rectified-linear units, except the last layer which has linear units. C denotes a convolutional layer with the number of filters and the filter size inscribed, FC a fully connected layer with the number of neurons, and UP an unpooling layer with the upscaling factor.
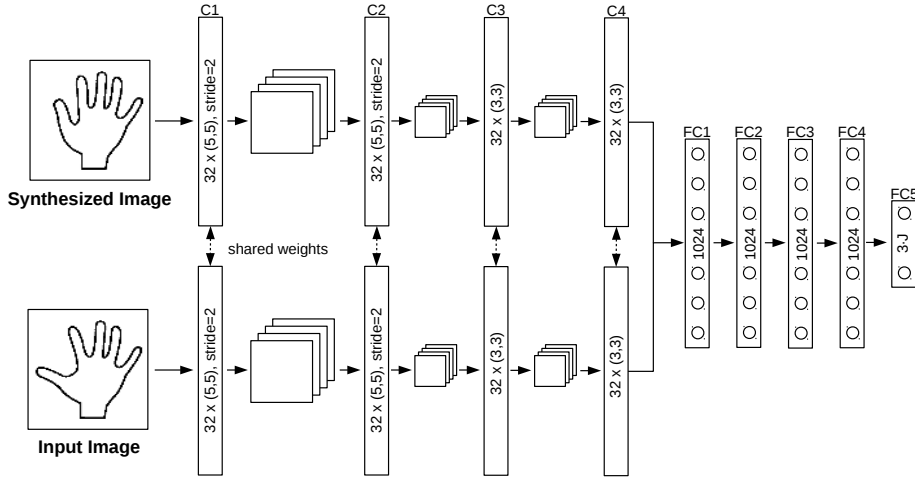


Figure 5: Architecture of the updater. The network consists of two identical paths with shared weights that contain several convolutional layers that use a filter stride to reduce the size of the feature maps. The final feature maps are concatenated and fed into a fully connected network. All layers have rectified-linear units, except the last layer which has linear units. The pose update is used to refine the initial pose and the refined pose is again fed into the synthesizer to iterate the whole procedure. As in Fig. 4, C denotes a convolutional layer, and FC a fully connected layer.

with small Gaussian noise for all poses. This creates convergence basins around the ground truth, in which the predicted updates point towards the ground truth, as we show in the evaluation, and further helps to explore the pose space.

After every 2 epochs, we further augment the set by applying the current updater to the poses in $\mathcal{T}_\mathcal{D}$, that is, we add the set

$$\{\mathbf{p}_2 \mid \exists \mathbf{p} \in \mathcal{T}_\mathcal{D} \text{ s.t. } \mathbf{p}_2 = \mathbf{p} + \text{updater}(\mathcal{D}, \text{synth}(\mathbf{p}))\} \tag{9}$$

to $\mathcal{T}_\mathcal{D}$. This forces the updater to learn to further improve on its own outputs.

In addition, we sample from the current distribution of errors across all the samples, and add these errors to the poses, thus explicitly focusing the training on common deviations. This is different from the Gaussian noise and helps to predict correct updates for larger initialization errors.

## 4. Evaluation

In this section we evaluate our proposed method on the NYU Hand Pose Dataset [35], a challenging real-world benchmark for hand pose estimation. First, we describe how we train the networks. Then, we introduce the evaluation metric and the benchmark dataset. Furthermore we evaluate our method qualitatively and quantitatively.

### 4.1. Training

We optimize the networks' parameters by using error back-propagation and apply the rmsprop [34] algorithm. We choose a decay parameter of $0.9$ and truncate the gradients to $0.01$. The batch size is $64$. The learning rate decays over the epochs and starts with $0.01$ for the predictor and synthesizer, and with $0.001$ for the updater. The networks are trained for $100$ epochs.

Figure 7: The effects of erroneous annotations in the training data of [30]. The figures show input images together with synthesized images which exhibit very blurry outlines and "ghost" fingers. The synthesizer learns the erroneous annotations and interpolates between inconsistent ones, causing such artifacts that limit the applicability in our method. (Best viewed on screen)

## 4.2. Hand Detection

We extract a fixed-size metric cube from the depth image around the hand. The depth values within the cube are resized to a $128 \times 128$ patch and normalized to $[-1, 1]$. The depth values are clipped to the cube sides front and rear. Points for which the depth is undefined—which may happen with structured light sensors for example—are assigned to the rear side. This preprocessing step was also done in [30] and provides invariance to different hand-to-camera distances.

## 4.3. Benchmark

We evaluated our method on the NYU Hand Pose Dataset [35]. This dataset is publicly available, it is backed up by a huge quantity of annotated samples together with very accurate annotations. It also shows a high variability of poses, however, which can make pose estimation challenging. While the ground truth contains $J = 36$ annotated joints, we follow the evaluation protocol of [21, 35] and use the same subset of $J = 14$ joints.

The training set contains samples of one person, while the test set has samples from two persons. The dataset was captured using a structured light RGB-D sensor, the Primesense Carmine 1.09, and contains over 72k training and 8k test frames. We used only the depth images for our experiments. They exhibit typical artifacts of structured light sensors: The outlines are noisy and there are missing depth values along occluding boundaries.

We also considered other datasets for this task; unfortunately, no further dataset was suitable. The dataset of Tang *et al*. [30] has large annotation errors, that cause blurry outlines and "ghost" fingers in the synthesized images as shown in Fig. 7, which are not suitable for our method. The datasets of [26, 29, 37] provide too little training data to train meaningful models.

## 4.4. Comparison with Baseline

We show the benefit of using our proposed feedback loop to increase the accuracy of the 3D joint localization. For this, we compare to Tompson *et al*. [35], and to Ober-

weger *et al*. [21]. For [35], we augment their 2D joint locations with the depth from the depth images, as done in [35]. In case this estimate is outside the hand cube we assign ground truth depth, thus favorably mitigating large errors in those cases. For [21], we use their best CNN that incorporates a 30D pose embedding.

The quantitative comparison is shown in Fig. 8a. It shows results using the metric of [33] which is generally regarded as being very challenging. It denotes the fraction of test samples that have all predicted joints below a given maximum Euclidean distance from the ground truth. Thus a single erroneous joint results in the deterioration of the whole hand pose.

While the baseline of [35] and [21] have an average Euclidean joint error of 21 mm and 20 mm respectively, our proposed method reaches an error reduction to 16.5 mm, thus achieving state-of-the-art on the dataset. The initialization with the simple and efficient proposed predictor has an error of 27 mm. We further show an evaluation of different initializations in Fig. 8b. When we use a more complex initialization [21] with an error of 23 mm, we can decrease the average error to 16 mm. For a more detailed breakdown of the error evaluation of each joint, we refer to the supplementary material.

## 4.5. Image-Based Hand Pose Optimization

We mentioned in Section 3.1 that the attempt may be made to estimate the pose by directly optimizing the squared loss between the input image and the synthetic one as given in Eq. (3) and we argued that this does not in fact work well. We now demonstrate this empirically.

We used the powerful L-BFGS-B algorithm [5], which is a box constrained optimizer, to solve Eq. (3). We set the constraints on the pose in such a manner that each joint coordinate stays inside the hand cube.

The minimizer of Eq. (3), however, does not correspond to a better pose in general, as shown in Fig. 9. Although the generated image looks very similar to the input image, the pose does not improve, moreover it even often becomes worse. Several reasons can account for this. The depth input image typically exhibits noise along the contours, as in the example of Fig. 9. After several iterations of L-BFGS-B, the optimization may start corrupting the pose estimate with the result that the synthesizer generates artifacts that fit the noise. As shown in Fig. 10, the pose after optimization is actually worse than the initial pose of the predictor.

Furthermore the optimization is prone to local minima due to a noisy error surface [26]. However, we also tried Particle Swarm Optimization [22, 26, 28] a genetic algorithm popular for hand pose optimization, and obtained similar results. This tends to confirm that the bad performance comes from the objective function of Eq. (3) rather than the optimization algorithm.
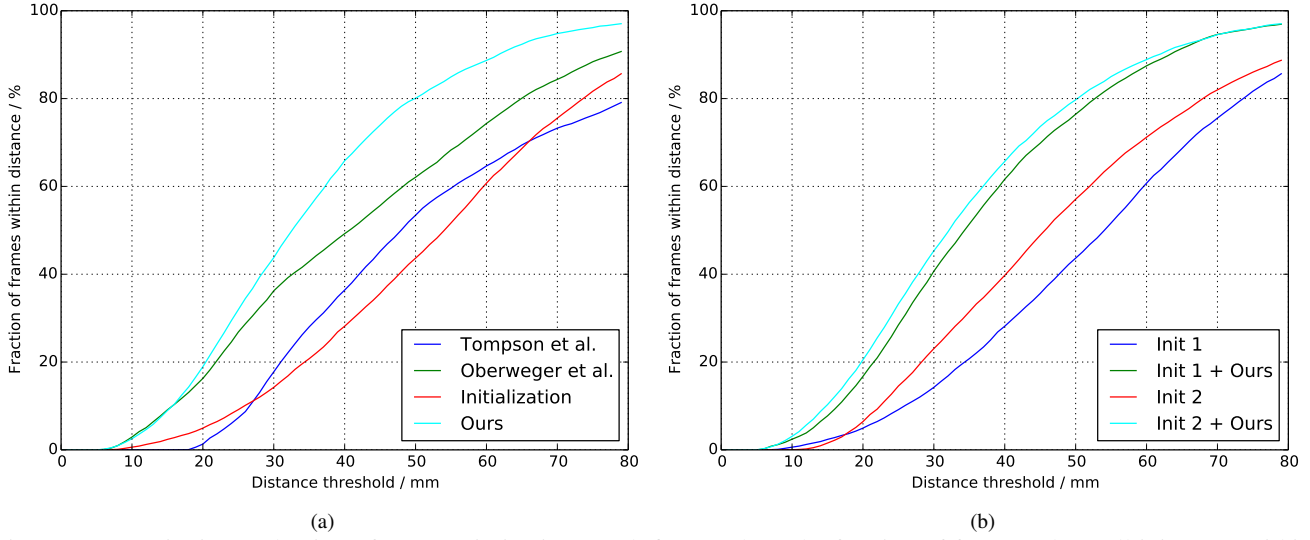
(a)



(b)

Figure 8: Quantitative evaluation of pose optimization. Both figures show the fraction of frames where all joints are within a maximum distance. A higher area under the curve denotes better results. In (a) we compare our method to the baseline of Tompson *et al.* [35] and Oberweger *et al.* [21]. Although our initialization is worse than both baselines, we can boost the accuracy of the joint locations using our proposed method. In (b) we compare different initializations. *Init 1* is the simple predictor presented in this work. We also use the more sophisticated model of [21], denoted as *Init 2*, for a more accurate initialization. The better initialization helps obtain slightly more accurate results, however, our much simpler and faster predictor is already sufficient for our method as initialization. (Best viewed on screen)
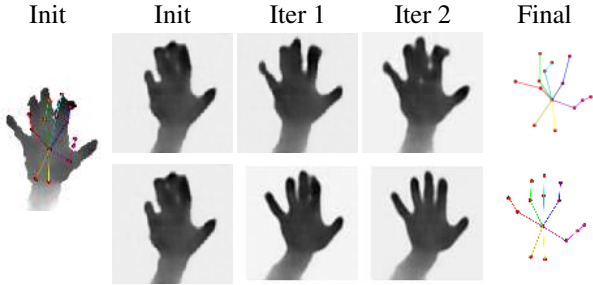


Figure 9: Comparison with image-based pose optimization. **(Top)** results for image-based optimization, and **(bottom)** for our proposed method. From left to right: input depth image with initial pose, synthesized image for initial pose, after first, second iteration, and final pose. Minimizing the difference between the synthesized and the input image does not induce better poses. Thanks to the updater, our method can fit a good estimate. (Best viewed on screen)

By contrast, in Fig. 12 we show the predicted updates for different initializations around the ground truth joint location with our updater. It predicts updates that move the pose closer to the ground truth, for almost all initializations.

### 4.6. Qualitative results

Fig. 11 shows some qualitative examples. For some examples, the predictor provides already a good pose, which we can still improve, especially for the thumb. For
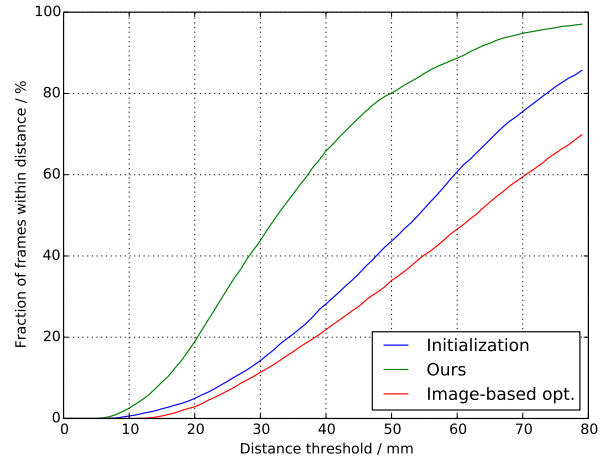


Figure 10: Comparing image-based optimization and our feedback loop. A higher area under the curve denotes better results. The image-based optimization actually tends to result in a deterioration of the initial pose estimate. Our proposed optimization method performs significantly better. (Best viewed in color)

worse initializations, also larger updates on the pose can be achieved by our proposed method, to better explain the evidence in the image.
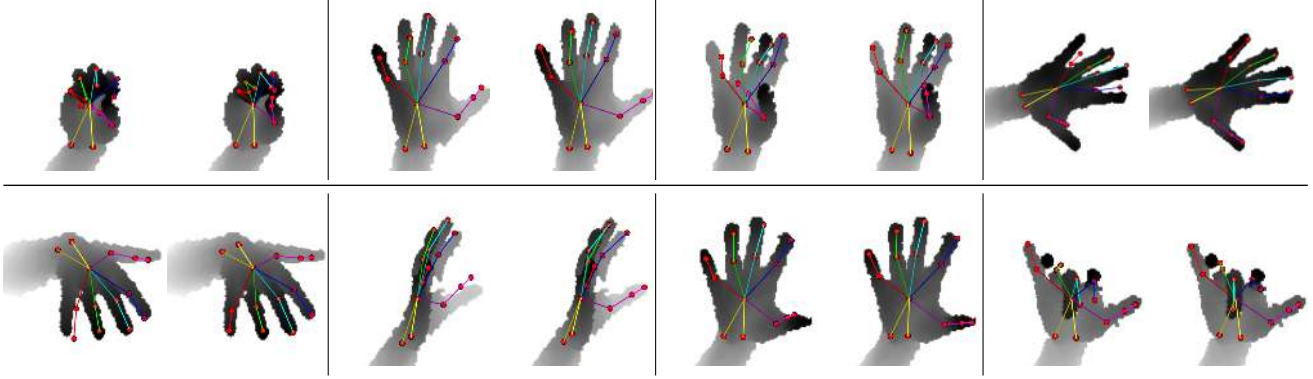
Figure 11: Qualitative results for NYU dataset. We show the inferred joint locations on the depth images where the depth is color coded in gray-scale. The individual fingers are color coded, where the bones of each finger share the same color, but with a different hue. The left image of each pair shows the initialization and the right image shows the pose after applying our method. Our method applies to a wide variety of poses and is tolerant to noise, occlusions and missing depth values as shown in several images. (Best viewed on screen)
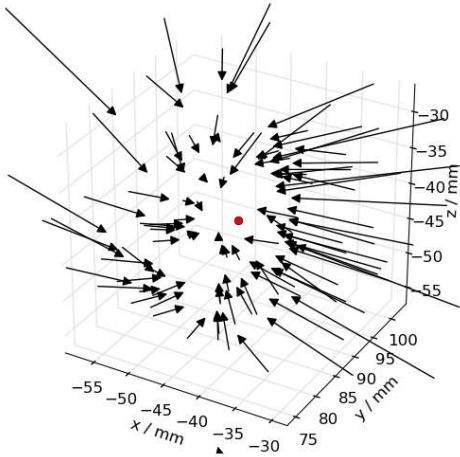


Figure 12: Predicted updates around ground truth joint position, denoted as ●. We initialize noisy joint locations around the ground truth location and show the pose updates as vectors predicted by our updater. The start and end of the vectors denote the initial and the updated 3D joint location. The different updates bring us closer to the ground truth joint location. (Best viewed on screen)

### 4.7. Runtime

Our method is implemented in Python using the Theano library [2] and we run the experiments on a computer equipped with an Intel Core i7, 16GB of RAM, and an nVidia GeForce GTX 780 Ti GPU. Training takes about ten hours for each CNN.

The runtime is composed of the discriminative initialization that takes 0.07 ms, the updater network takes 1.2 ms for each iteration, and that already includes the synthesizer with 0.8 ms. In practice we iterate our updater twice, thus our method performs very fast at over 400 fps on a single GPU. The runtime of our method compares favorably with other model-based methods ranging between 12 and 60 fps [19, 22, 26, 29, 37].

## 5. Discussion and Conclusion

While our approach is not really biologically-inspired, it should be noted that similar feedback mechanisms also have the support of strong biological evidence. It has been shown that feedback paths in the brain and especially in the visual cortex actually consist of *more* neurons than the forward path [7]. Their functional role remains mostly unexplained [4]; our approach could be a possible explanation in the case of feedback in the visual cortex, but of course, this would need to be proved.

It should also be noted that our predictor and our synthesizer are trained with exactly the same data. One may then ask how our approach can improve the first estimate made by the predictor. The combination of the synthesizer and the updater network provides us with the possibility for simply yet considerably augmenting the training data to learn the update of the pose: For a given input image, we can draw arbitrary numbers of samples of poses through which the updater is then trained to move closer to the ground-truth. In this way, we can explore regions of the pose space which are not present in the training data, but might be returned by the predictor when applied to unseen images.

Finally, our approach has nothing really specific to the hand pose detection or the use of a depth camera, since all its components are learned, from the prediction of the initialization to the generation of images and the update computation. The representation of the pose itself is also very simple and does not have to take into account the specifics of the structure of the hand. We therefore believe that, given proper training data, our approach can be applied to many detection and tracking problems and also with different sensors.

# References

[1] L. Ballan, A. Taneja, J. Gall, L. V. Gool, and M. Pollefeys. Motion Capture of Hands in Action Using Discriminative Salient Points. In *ECCV*, 2012.

[2] J. Bergstra, O. Breuleux, F. Bastien, P. Lamblin, R. Pascanu, G. Desjardins, J. Turian, D. Warde-Farley, and Y. Bengio. Theano: A CPU and GPU Math Expression Compiler. In *Proc. of SciPy*, 2010.

[3] C. Bishop. *Pattern Recognition and Machine Learning*. Springer, 2006.

[4] F. Briggs and W. Usrey. Emerging Views of Corticothalamic Function. *Current Opinion in Neurobiology*, 2008.

[5] R. H. Byrd, P. Lu, J. Nocedal, and C. Zhu. A Limited Memory Algorithm for Bound Constrained Optimization. *SIAM Journal on Scientific and Statistical Computing*, 16(5), 1995.

[6] S. Chopra, R. Hadsell, and Y. LeCun. Learning a Similarity Metric Discriminatively, with Application to Face Verification. In *CVPR*, 2005.

[7] P. Dayan and L. Abbott. *Theoretical Neuroscience: Computational and Mathematical Modeling of Neural Systems*. MIT Press, 2005.

[8] M. de La Gorce, D. J. Fleet, and N. Paragios. Model-Based 3D Hand Pose Estimation from Monocular Video. *PAMI*, 33(9), 2011.

[9] A. Dosovitskiy, J. T. Springenberg, and T. Brox. Learning to Generate Chairs with Convolutional Neural Networks. In *CVPR*, 2015.

[10] A. Erol, G. Bebis, M. Nicolescu, R. D. Boyle, and X. Twombly. Vision-Based Hand Pose Estimation: A Review. *CVIU*, 108(1-2), 2007.

[11] I. J. Goodfellow, J. Pouget-Abadie, M. Mirza, B. Xu, D. Warde-Farley, S. Ozair, A. Courville, and Y. Bengio. Generative Adversarial Nets. In *NIPS*, 2014.

[12] A. Jain, J. Tompson, M. Andriluka, G. W. Taylor, and C. Bregler. Learning human pose estimation features with convolutional networks. In *Proc. of ICLR*, 2014.

[13] C. Keskin, F. Kıraç, Y. E. Kara, and L. Akarun. Real Time Hand Pose Estimation Using Depth Sensors. In *ICCV*, 2011.

[14] C. Keskin, F. Kıraç, Y. E. Kara, and L. Akarun. Hand Pose Estimation and Hand Shape Classification Using Multi-Layered Randomized Decision Forests. In *ECCV*, 2012.

[15] T. D. Kulkarni, W. Whitney, P. Kohli, and J. B. Tenenbaum. Deep Convolutional Inverse Graphics Network. In *NIPS*, 2015.

[16] T. D. Kulkarni, I. Yildirim, P. Kohli, W. A. Freiwald, and J. B. Tenenbaum. Deep Generative Vision as Approximate Bayesian Computation. In *NIPS*, 2014.

[17] A. Kuznetsova, L. Leal-taixe, and B. Rosenhahn. Real-Time Sign Language Recognition Using a Consumer Depth Camera. In *ICCV*, 2013.

[18] S. Liu, X. Liang, L. Liu, X. Shen, J. Yang, C. Xu, L. Lin, X. Cao, and S. Yan. Matching-CNN Meets KNN: Quasi-Parametric Human Parsing. In *CVPR*, 2015.

[19] S. Melax, L. Keselman, and S. Orsten. Dynamics Based 3D Skeletal Hand Tracking. In *Proc. of Graphics Interface Conference*, 2013.

[20] V. Nair, J. Susskind, and G. E. Hinton. Analysis-By-Synthesis by Learning to Invert Generative Black Boxes. In *Proc. of ICANN*, 2008.

[21] M. Oberweger, P. Wohlhart, and V. Lepetit. Hands Deep in Deep Learning for Hand Pose Estimation. In *Proc. of CVWW*, 2015.

[22] I. Oikonomidis, N. Kyriazis, and A. A. Argyros. Efficient Model-Based 3D Tracking of Hand Articulations Using Kinect. In *BMVC*, 2011.

[23] I. Oikonomidis, N. Kyriazis, and A. A. Argyros. Full DOF Tracking of a Hand Interacting with an Object by Modeling Occlusions and Physical Constraints. In *ICCV*, 2011.

[24] R. Plänkers and P. Fua. Articulated Soft Objects for Multi-View Shape and Motion Capture. *PAMI*, 25(10), 2003.

[25] PrimeSense. Primesense 3D Sensors, 2015.

[26] C. Qian, X. Sun, Y. Wei, X. Tang, and J. Sun. Realtime and Robust Hand Tracking from Depth. In *CVPR*, 2014.

[27] D. Scherer, A. Müller, and S. Behnke. Evaluation of Pooling Operations in Convolutional Architectures for Object Recognition. In *Proc. of ICANN*, 2010.

[28] T. Sharp, C. Keskin, D. Robertson, J. Taylor, J. Shotton, D. Kim, C. Rhemann, I. Leichter, A. Vinnikov, Y. Wei, D. Freedman, P. Kohli, E. Krupka, A. Fitzgibbon, and S. Izadi. Accurate, Robust, and Flexible Real-Time Hand Tracking. In *Proc. of CHI*, 2015.

[29] S. Sridhar, A. Oulasvirta, and C. Theobalt. Interactive Markerless Articulated Hand Motion Tracking Using RGB and Depth Data. In *ICCV*, 2013.

[30] D. Tang, H. J. Chang, A. Tejani, and T.-K. Kim. Latent Regression Forest: Structured Estimation of 3D Articulated Hand Posture. In *CVPR*, 2014.

[31] D. Tang, T. Yu, and T. Kim. Real-Time Articulated Hand Pose Estimation Using Semi-Supervised Transductive Regression Forests. In *ICCV*, 2013.

[32] Y. Tang, N. Srivastava, and R. Salakhutdinov. Learning Generative Models with Visual Attention. In *NIPS*, 2014.

[33] J. Taylor, J. Shotton, T. Sharp, and A. Fitzgibbon. The Vitruvian Manifold: Inferring Dense Correspondences for One-Shot Human Pose Estimation. In *CVPR*, 2012.

[34] T. Tieleman and G. Hinton. Lecture 6.5-Rmsprop: Divide the Gradient by a Running Average of Its Recent Magnitude. *COURSERA: Neural Networks for Machine Learning*, 2012.

[35] J. Tompson, M. Stein, Y. LeCun, and K. Perlin. Real-Time Continuous Pose Recovery of Human Hands Using Convolutional Networks. *ACM Transactions on Graphics*, 33, 2014.

[36] D. Tzionas, A. Srikantha, P. Aponte, and J. Gall. Capturing Hand Motion with an RGB-D Sensor, Fusing a Generative Model with Salient Points. In *Proc. of GCPR*, 2014.

[37] C. Xu and L. Cheng. Efficient Hand Pose Estimation from a Single Depth Image. In *ICCV*, 2013.

[38] M. D. Zeiler and R. Fergus. Visualizing and Understanding Convolutional Networks. In *ECCV*, 2014.

[39] M. D. Zeiler, G. W. Taylor, and R. Fergus. Adaptive Deconvolutional Networks for Mid and High Level Feature Learning. In *ICCV*, 2011.